Available online at www.sciencedirect.com
SCIENCE DIRECT®
Physica B 336 (2003) 204–210
PHYSICA B
www.elsevier.com/locate/physb

Lipophilic C_{60}-derivative-induced structural changes in phospholipid layers

U. Jeng[a,c], T.-L. Lin[a,*], K. Shin[b], C.-H. Hsu[c], H.-Y. Lee[c], M.H. Wu[d], Z.A. Chi[d], M.C. Shih[d], L.Y. Chiang[e]

[a] *Department of Engineering and System Science, National Tsing Hua University, Hsinchu 300, Taiwan*
[b] *Department of Materials Science and Engineering, Kwangju Institute of Science and Technology, Kwangju, South Korea*
[c] *Synchrotron Radiation Research Center, Hsinchu 300, Taiwan*
[d] *Department of Physics, National Chung-Hsin University, Tai-Chung 402, Taiwan*
[e] *Center for Condensed Matter Sciences, National Taiwan University, Taipei 106, Taiwan*

Received 26 September 2002; accepted 6 January 2003

Abstract

We have studied the interactions of a lipophilic C_{60}-derivative, synthesized recently for potential biomedical applications, with phospholipid monolayers and bilayers. The results of surface pressure–area isotherms, atomic force microscopic images, and neutron and X-ray scattering show consistently that the lipophilic C_{60} can intercalate into monolayers as well as vesicle bilayers of the phospholipids studied. In general, the lipophilic C_{60} can incorporate into the lipid membranes better in the liquid crystal phase, and modify the bending and compression modulus of the host lipid membranes significantly.
© 2003 Elsevier Science B.V. All rights reserved.

Keywords: Lipophilic fullerenes; Phospholipid layers; Neutron reflection; SAXS

1. Introduction

There are large activities in studying interactions of lipid membranes with many different membrane intruders, for instances, peptides [1], disaccharides [2], or enzymes [3], etc. Although these intruders interact with lipid membranes for different purposes, such as attacking, protecting, or function attaching, a common preceding action for all shall be a binding to the lipid membranes. Regarding the cell protecting effect, C_{60} has demonstrated an outstanding performance due to its capability of eliminating radicals in biosystems [4]. Nevertheless, the binding efficiency to lipid membranes or bilayers is very limited due to the strong aggregation behavior of C_{60}. To circumvent the small solubility of C_{60} in lipid membranes, we have synthesized a lipophilic C_{60} derivative, FPTL, having three lipid-like tails chemically bonded on one olefinic moiety of the C_{60} cage. With the three lipid-like tails simulating largely the molecular structure of a phospholipid, dipalmitoylphosphatidylcholine (DPPC), the lipophilic C_{60} is ready to incorporate into phospholipid membranes.

Here, we study the interactions of FPTL with DPPC monolayers and bilayers basing mainly on the FPTL-induced structural changes in the host

*Corresponding author.
E-mail address: tllin@mx.nthu.edu.tw (T.-L. Lin).

0921-4526/03/$ - see front matter © 2003 Elsevier Science B.V. All rights reserved.
doi:10.1016/S0921-4526(03)00290-4

entities. In the following, we detail the structural characterization for the DPPC/FPTL mixing system using surface pressure–area ($\pi-A$) isotherms, neutron and X-ray scattering, as well as atomic force microscopy (AFM).

2. Experimental

Fig. 1 shows the schematic view of the lipophilic C_{60}, FPTL, of a molecular weight M_w of 2178. The detailed synthesis route for FPTL will be reported elsewhere. We dissolved deuterated DPPC (d_{62}-DPPC, two acyle chains deuterated, $M_w = 796$, see Fig. 1) and FPTL (6.3% molar ratio of DPPC) into a mixing solvent of benzene and chloroform (2:1 volume ratio). The use of deuterated lipids is to increase the scattering sensitivity for neutrons. The sample solution was used in forming Langmuir films for isotherm and neutron reflection measurements, respectively. For SAXS sample solutions, we mixed regular (non-deuterated) DPPC and FPTL with 50:1 molar ratio in an organic solvent (dichlorobenzene and dimethyl sulfoxide). The mixture was vacuum-dried into powders, and subsequently dissolved into water and ultrasonicated into a 10 mM solution of DPPC/FPTL vesicles. For comparison, a pure DPPC vesicle solution was also prepared with the same concentration.

Surface pressure isotherms were observed with a slow compression speed of 8 cm^2/min on a NIMA Langmuir trough of an area of 500 cm^2, where LB films are prepared for AFM and in-plane X-ray scattering. With a vertical dipping method, LB films were transferred onto mica substrates, of dimensions of $2.5 \times 7\,cm^2$, where each half of the mica surface was preserved for scattering background measurement. Neutron reflectivity measurements were conducted on another Langmuir trough incorporated into the NG7 neutron reflectometer [5] at the National Institute of Standards

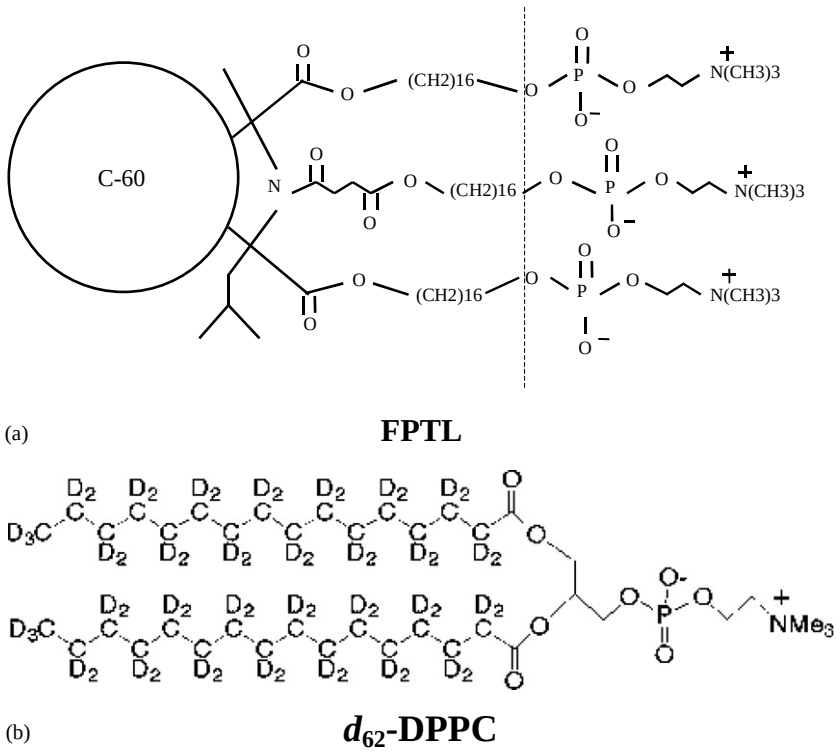

Fig. 1. Schematic view for the lipophilic C_{60}, FPTL, and d_{62}-DPPC. For FPTL, the dotted line separates the hydrophobic part, C_{60} + lipid chains, and the hydrophilic part, phosphate lipid heads.

and Technology (NIST). We used a neutron beam of 4.76 Å wavelength, with the beam width fixed at 25 mm and the beam height adjusted according to the Q value scanned for a constant Q resolution of 3%. The scattering wave vector transfer $Q = 4\pi \sin(\theta)/\lambda$ is defined by the scattering angle 2θ and the wavelength λ of the radiation quanta.

X-ray scattering measurements were conducted on a setup basing on an 8-circle diffractometer of the wiggler beam line BL17B in the Synchrotron Radiation Research Center (SRRC) of Taiwan, as detailed in Ref. [6]. We used a double-crystal monochromator (DCM) of Si(1 1 1) for a beam of a wavelength λ of 1.55 Å in this study. The beam was collimated by two sets of slits, 0.4×0.4 and $0.4 \times 0.6\,mm^2$, separated by 1 m, which results in a photon flux $\sim 10^9$ photons/s at the sample position. With the mechanics of the 8-circle diffractometer, we could position and align the sample and detector for in-plane GISAXS as well as specular reflection measurements. Two detectors, a scintillation counter and a position sensitive linear detector located 815 and 960 mm from the sample position, respectively, were used for reflectivity and GISAXS measurements. The X-ray scattering setup gave an angular resolution of 0.028° and 0.006°, or 0.004 and $0.001\,Å^{-1}$ for the Q resolution, in the vertical and horizontal directions, respectively. For all GISAXS measurements, the incident angles were fixed at 0.225°, or $Q_z = 0.032\,Å^{-1}$, which was slightly smaller than the critical angle for the total reflection of the mica substrates.

3. Results

3.1. Interactions of DPPC and FPTL in Langmuir monolayers

The surface pressure–area ($\pi - A$) isotherms of a Langmuir film characterize the mechanical properties of the film, such as compressibility and stability, that relate to the detail interactions between the film molecules themselves and the film molecules with water, the subphase. In Fig. 2, the bizarre $\pi - A$ isotherms (squares), compression and decompression, measured at 20°C for the

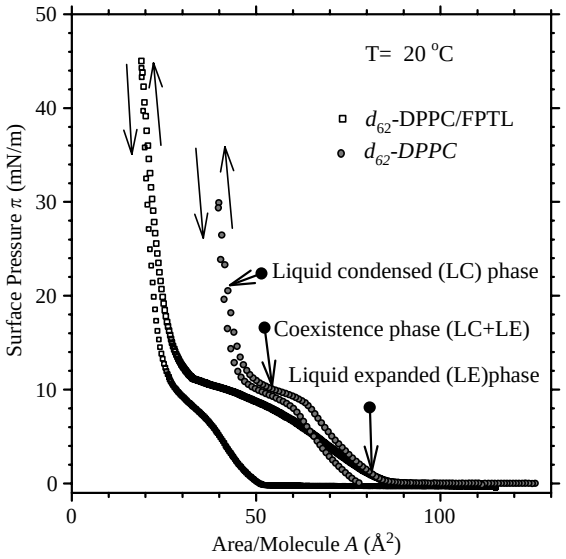

Fig. 2. Compression (arrow up) and decompression (arrow down) isotherms measured at 20 °C for the d_{62}-DPPC/FPTL and d_{62}-DPPC Langmuir films.

DPPC/FPTL Langmuir film are quite informative. Compared to the pure DPPC isotherms (circles), which have a well-defined plateau at $\pi \sim 10$ mN/m for the coexistence phase [7], the mixture layer does not display a clear coexistence phase. Together with the large hysteresis and smaller A (area per molecule) for the liquid condensed (LC) phase observed, apparently, the lateral packing of DPPC molecules in the air–water interface is strongly influenced by the presence of small amount of FPTL molecules. An aggregation induced by FPTL in the DPPC/FPTL Langmuir film may explain these isotherms characteristics observed. The possible aggregates might be mesoscaled and weakly bounded, since the isotherm is reproducible essentially after a recompression, and the hysteresis is much smaller in the LC phase.

The possible induced aggregation by FPTL is also hinted by the AFM images of the DPPC/FPTL LB films. For the DPPC/FPTL LB films prepared in the liquid expanded (LE) phase ($\pi = 3$ mN/m), the AFM images exhibit aggregation domains that do not exist in pure DPPC LB films [8]. On the other hand, the AFM images

observed (Fig. 3) for the DPPC/FPTL LB films prepared in the LC phase ($\pi = 30\,\mathrm{mN/m}$) show much less voids (defects) than that for pure DPPC LB films prepared under the same conditions. This implies that FPTL can improve the integrity of the LB film for a more homogeneous morphology through, presumably, FPTL-induced aggregation or coalescence.

Using the grazing incidence SAXS technique, we, furthermore, explore the in-plane structure of the DPPC/FPTL and the pure DPPC LB films, prepared at the LC phase ($\pi = 30\,\mathrm{mN/m}$). In Fig. 4, the DPPC/FPTL LB film exhibits a substantial excess scattering than that for the DPPC LB film. Since the thickness, $\sim 26\,\text{Å}$, for both LB films, determined by X-ray reflectivity, is compatible to

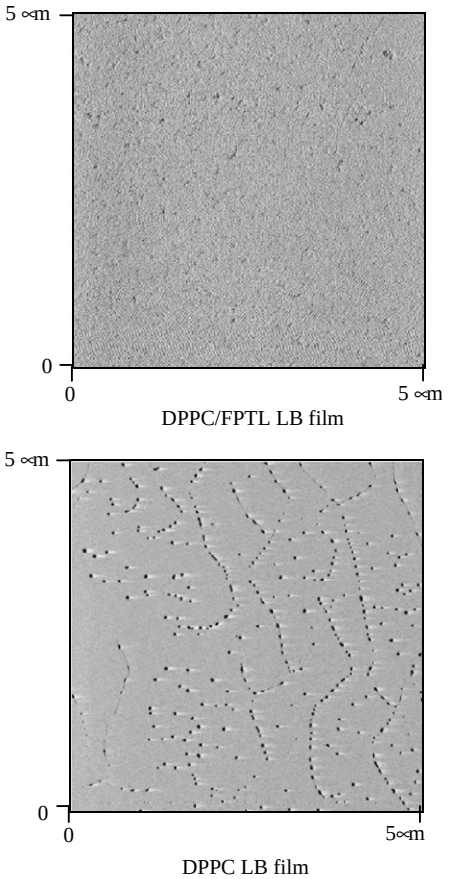

Fig. 3. AFM images, $5 \times 5\,\mu\mathrm{m}^2$, for the DPPC/FTPL and DPPC LB films, prepared in the LC phase ($\pi = 30\,\mathrm{mN/m}$).

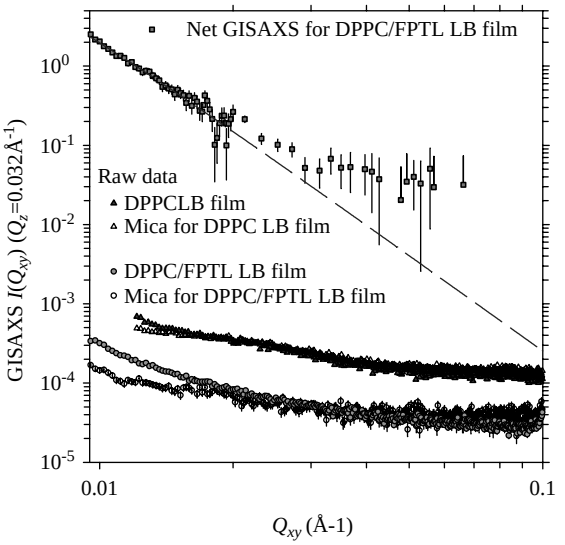

Fig. 4. Grazing incidence SAXS for the DPPC/FPTL (solid circles) LB film on mica and mica substrate (empty circles), also the DPPC (solid triangles) LB film and its mica substrate (empty triangles). The net GISAXS data (squares) for the DPPC/FPTL film, with the scattering from mica subtracted, are rescaled and fitted (dashed curve) with a Debye–Buche model. Q_{xy} is the in-plane wave vector transfer. For all measurements, the incident angles were fixed at 0.225 ° ($Q_z = 0.032\,\text{Å}^{-1}$).

the size of a DPPC monolayer, we attribute the excess in-plane scattering of the DPPC/FPTL LB film to the in-plane local density fluctuations induced by FPTL in the mixture monolayer. Using the Debye–Buche model, we fit (dashed curve in Fig. 4) the in-plane scattering intensity with $I(Q) \propto (1 + Q^2\xi^2)^{-2}$ [6], where an in-plane correlation length $\xi = 270 \pm 30\,\text{Å}$ can be extracted. The correlation length implies a loose in-plane ordering in the DPPC/FPTL monolayer, which, likely, corresponds to the interaction range of FPTL in the monolayer. The existence of the mesoscaled ordering (or aggregates) may be responsible for the large hysteresis in the isotherms observed (see Fig. 2) for the DPPC/FPTL Langmuir monolayer.

For subtle interactions between DPPC and FTPL at the air–water interface, we use neutron reflectivity with a selected deuteration on DPPC lipids chains for a highlight [9]. The neutron reflection data (Fig. 5a) for the pure DPPC Langmuir layer on H_2O surface measured at the gel (20°C) and liquid crystal (50°C) phases of

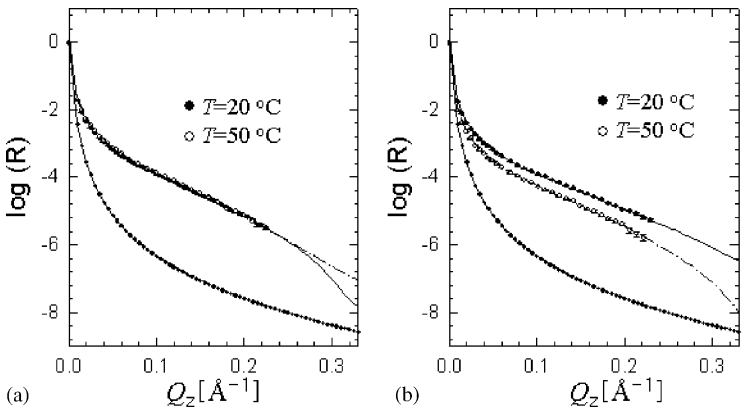

Fig. 5. In situ neutron reflectivity data for the (a) d_{62}-DPPC and (b) d_{62}-DPPC/FTPL Langmuir layers at the air–water(H_2O) interface. The lowest curves (cross) in both sets are simulated reflectivity curves for H_2O. The solid and dashed curves are the least-squares fits for the reflectivity data measured at 20 °C and 50°C, respectively, for each system.

DPPC [10], respectively, show that the fully stretched aliphatic chains in gel phase melt from 18 Å to a smaller layer thickness of 17 Å, when temperature rises to the liquid crystal phase. This is a usual case [10]. On the other hand, neutron reflection data (Fig. 5b) for the DPPC/FPTL Langmuir monolayer display an amazing film stiffening effect. Specifically, in the FPTL-incorporated DPPC monolayer, the aliphatic chains do not melt when temperature rises to the liquid crystal phase. Instead, the chains stretch out more for a lager layer thickness (from 15–18 Å). (See Table 1. Detailed neutron data analysis will be reported elsewhere [11].) We attribute this phenomenon observed to the buckling effect of FPTL on the DPPC molecules in the monolayer, via the relatively long-ranged interactions of FPTL. Elaborately, when temperature rises to the liquid crystal phase, the packing of DPPC looses up for a larger surface area A [10], which allows the bulkier FPTL (three lipid tails in one FPTL, see Fig. 1) locking into DPPC film better, and pushing the aliphatic chains of DPPC molecules from their preferred 35° tilt to an upright position [3]. The similar effect was also observed by Dahmen-Levison et al. [12] in a system, where the intercalated molecules introduced strong hydrophobic interactions into the chain regions of DPPC monolayers, thus overrode the hydrophilic anchoring power of DPPC heads in water causing the 35° tilt chain conformation. Surely, in our case, the C_{60} anchored on FPTL is famous for the strong hydrophobicity and C_{60}–C_{60} interactions. Interestingly, we have also observed the same buckling effect of FPTL on DPPC molecules in the FPTL-intercalated vesicle bilayers, as detailed in the following.

3.2. Interactions of DPPC and FPTL in solution bilayers

In Figs. 6 and 7, we show the SAXS results for the DPPC/FPTL and pure DPPC vesicles, measured in the gel ($T \lesssim 25$°C), ripple ($T \sim 39$°C), and liquid crystal ($T \gtrsim 45$°C) phases of pure DPPC, respectively [13]. In the gel phase, $A = 48$ Å^2 [10], the SAXS data (Fig. 6, 22°C) for the pure DPPC vesicles show a relatively sharp peak at $Q_c = 0.0916$ Å^{-1}, corresponding to a bilayers spacing $d(= Q_c/2\pi)$ of 68.6 Å. The peak is damped significantly due to the intercalation of FPTL (Fig. 7, 22°C). As temperature rises to the ripple phase, the scattering peak of the bilayers ordering for the pure DPPC vesicles is washed out by thermal fluctuations (Fig. 6, 42°C);[1] whereas the DPPC/

[1] Since SAXS intensity comes mainly from the phosphate groups of the lipid heads of ~5 Å thick. The SAXS scattering peak is sensitive or vulnerable to the interface roughness imposed by thermal fluctuations.

Table 1
Fitting parameters for the NR data shown in Fig. 5

Sample	Temp. (°C)	SLD_{head} ($10^{-6} \times Å^{-2}$)	d_{head} (Å)	$\sigma_{head-tail}$ (Å)	SLD_{tail} ($10^{-6} \times Å^{-2}$)	d_{tail} (Å)
d_{62}-DPPC	20	0.8	7	3	4.8	18
	50	0.8	7	3	5.1	17
d_{62}-DPPC/FPTL	20	0.8	7	3	5.6	15
	50	0.8	7	3	3.3	18

A two-layer model for the scattering–length–density (SLD) profiles of the d_{62}-DPPC and d_{62}-DPPC/FPTL Langmuir films, corresponding to the head (d_{head}) and tail (d_{tail}) layers of the lipids, respectively, is used in the fitting algorithm. The transition width between the two layers is represented by $\sigma_{head-tail}$.

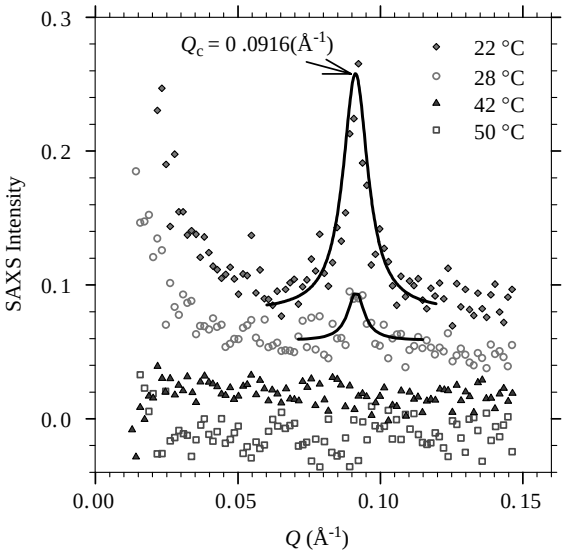

Fig. 6. SAXS data for the pure DPPC vesicles in water. The data for each temperature are rescaled for clarity. The data for 22°C and 28°C are fitted with Lorentzian curves (solid curves).

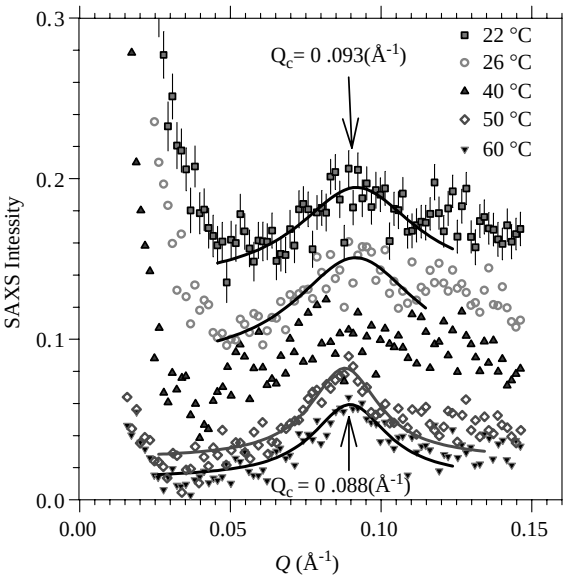

Fig. 7. SAXS data for the FPTL-intercalated DPPC vesicles in water. The data are rescaled for clarity and fitted (solid curves) with a Lorentzian function.

FPTL vesicles grasp a more ordered structure, as indicated by the scattering peak at 0.05 $Å^{-1}$ and a halo centered around 0.08 $Å^{-1}$ in Fig. 7 (40°C). The two peaks correspond to an in-plane ripple ordering and a bilayers ordering [13], respectively. When temperature increases further to the liquid crystal phase, the SAXS (Fig. 6, 50°C) for the DPPC vesicles remains structureless flat, whereas the SAXS (Fig. 7, 50°C) for the DPPC/FPTL vesicles manifests an even shaper peak for an unprecedented bilayer ordering in the system. The scattering peak persists at an even higher temperature, 60°C, of larger thermal fluctuations.

The temperature-dependent evolution of the bilayers scattering peak of DPPC/FPTL vesicles observed is reversible for temperature change. It narrates the history of FPTL's seizing control power on the host bilayers' structures and properties. In the beginning for the gel phase, FTPL molecules cannot intercalate into DPPC bilayers without disrupting the host's bilayers ordering, due to, presumably, their bulkier hydrophobic sides (C_{60} with three chains) of a packing conformation differing slightly from the tightly packed stiff chains of DPPC in the gel phase. In the liquid crystal phase finally reached, the

softened chains and a larger A ($=64\,\text{Å}^2$) for DPPC in this phase [10] helps FPTL to fit into the lipid bilayers easier and better. In fact, FPTL molecules not only incorporate into the DPPC bilayers for a better-ordered structure, but also protect this ordered structure from being destructed by thermal fluctuations. This implies stiffer bilayers for DPPC/FPTL vesicles than pure DPPC vesicles.[2] The slightly larger bilayers thickness, 71 Å ($Q_c = 0.088\,\text{Å}^{-1}$), may be a consequence of this stiffening effect of FPTL on the host's bilayers ($d = 67$ Å for pure DPPC bilayers in this phase [10]). The result echoes the stiffening effect observed by the neutron reflection measurement described previously for the Langmuir monolayers of DPPC/FPTL.

4. Conclusion

We have observed the interactions between the lipophilic C_{60}-derivative FPTL and DPPC from several different views. It is clear that FPTL molecules can bind into the phospholipid monolayers or bilayers studied and behave collectively with the lipid membranes. One of the dynamic consequences should be the increase of the bending and/or compression modulus of the host lipid membranes. It will be interesting to measure the change of bending energy in the FPTL-intercalated lipid bilayers, using, for instance, inelastic neutron scattering or spin-echo neutron scattering for the small energy change, of an order of thermal energy, $k_b T$.

[2] Note that the thermal fluctuations effect for the lipid bilayers in bulk water is much more serious than that for oriented bilayers on substrates. In the later, thermal fluctuations are strongly damped by the highly unbalanced pressures at the substrate interface, as also explained in Ref. [10].

Acknowledgements

We acknowledge the support of the National Institute of Standards and Technology for the use of the neutron reflectometer. This work was supported by the National Science Council, Grant NSC91-2113-M-007-037 (T.-L. Lin).

References

[1] M.H. Gaber, M.M. Ghanam, S.A. Ali, W.A. Khalil, Biophys. Chem. 70 (1998) 233.
[2] T. Hasegawa, J. Nishijo, J. Umemura, J. Phys. Chem. 102 (1998) 8498.
[3] U. Dahmen-Levison, G. Brezesinski, H. Mohwald, Thin Solid Films 327 (1998) 616.
[4] I.-C. Wang, L.A. Tai, D.D. Lee, P.P. Kanakamma, C.K.-F. Shen, T.-Y. Luh, C.H. Cheng, K.C. Hwang, J. Med. Chem. 42 (1999) 4614.
[5] A. Karim, J.F. Douglas, F. Horkay, L.J. Fetters, S.K. Satija, Physica B 221 (1996) 331.
[6] C.-H. Hsu, H.-Y. Lee, K.S. Liang, U. Jeng, D. Windover, T.M. Lu,C. Jin, Mat. Res. Soc. Symp. Proc. 612 (2002) D5.23.1.
[7] M.C. Petty, Langmuir–Blodgett Films, Cambridge University Press, New York, 1996.
[8] Z.A. Chi, M.C. Shih, Thesis published by National Chung-Hsin University, Taiwan.
[9] I.P. Purcell, J.R. Lu, R.K. Thomas, A.M. Howe, J. Penfold, Langmuir 14 (1998) 1637.
[10] J.F. Nagle, S. Tristram-Nagle, Biochim. Biophys. Acta 1469 (2000) 159.
[11] J.S. Koo et al., Int. J. Nanoscience, in press.
[12] U. Dahmen-Levison, G. Brezesinski, H. Mohwald, Colloids Surf. A: Physicochem. Eng. Aspects 171 (2000) 97.
[13] P.C. Mason, B.D. Gaulin, R.M. Epand, G.D. Wignall, J.S. Lin, Phys. Rev. E 59 (1999) 921.